The mechanical property and corrosion resistance of Mg-Zn-Nd alloy fine wires *in vitro* and *in vivo*

Ming Gao[a,b], Di Na[c], Xiangqiao Ni[c], Lihui Song[c], Iniobong P. Etim[a,b], Ke Yang[b], Lili Tan[b,*], Zheng Ma[b,**]

[a] School of Materials Science and Engineering, University of Science and Technology of China, Shenyang, 110016, China
[b] Institute of Metal Research, Chinese Academy of Sciences, Shenyang, 110016, China
[c] The First Hospital of China Medical University, Department of Surgical Oncology, China

ABSTRACT

Titanium and its alloy are commonly used as surgical staples in the reconstruction of intestinal tract and stomach, however they cannot be absorbed in human body, which may cause a series of complications to influence further diagnosis. Magnesium and its alloy have great potential as surgical staples, because they can be degraded in human body and have good mechanical properties and biocompatibility. In this study, Mg-2Zn-0.5Nd (ZN20) alloy fine wires showed great potential as surgical staples. The ultimate tensile strength and elongation of ZN20 alloy fine wires were 248 MPa and 13%, respectively, which could be benefit for the deformation of the surgical staples from U-shape to B-shape. The bursting pressure of the wire was about 40 kPa, implying that it can supply sufficient mechanical support after anastomosis. Biochemical test and histological analysis illustrated good biocompatibility and biological safety of ZN20 alloy fine wire. The residual tensile stress formed on the outside of ZN20 fine wire during drawing would accelerate the corrosion. The second phase had a negative influence on corrosion property due to galvanic corrosion. The corrosion rate *in vitro* was faster than that *in vivo* due to the capsule formed on the surface of ZN20 alloy fine wire.

1. Introduction

Titanium and titanium alloy surgical staples are widely used to anastomose the tissue during the reconstruction of intestinal tract and stomach due to stable chemical properties, no toxicity, good biocompatibility and enough mechanical properties [1,2]. However, the residues of titanium surgical staples can still cause some problems, such as affecting the medical diagnosis by computed tomography (CT) technique, causing anastomotic stenosis, secondary infection, bleeding and other complications. As an essential nutriment in the human body, magnesium and its alloys possess excellent biocompatibility, good mechanical properties and can completely degrade in human body [3–6]. Therefore, magnesium and its alloy show great application potentials as surgical staples to replace the titanium.

Many studies have already shown the application potentials of magnesium and its alloy as biodegradable implants, such as bone fixation, cardiovascular stent, surgical staples and microclip [7–12]. The biofunctions of magnesium have also been proved such as

stimulating bone growth, promoting angiogenesis and wound healing [13–15]. Wu et al. found good biocompatibility and no inflammation of pure magnesium staples that were implanted in stomach of pigs for 9 weeks [4]. The potential of magnesium alloy as surgical staples was also investigated by Cao et al. [16]. The magnesium alloy staples were implanted in beagles by gastrojejunal and colonic anastomosis, the wound healed well, and the staples degraded completely after 90 days.

Most studies on biodegradable magnesium based materials were pure magnesium and commercial magnesium alloys, such as AZ series alloys [17–19]. The mechanical property of pure magnesium is insufficient for applications in load-bearing. Although the mechanical property of AZ31 alloy is better than pure magnesium, Al can be harmful for neurons and will cause dementia and Alzheimer's disease [20,21]. Therefore, Al is not an appropriate alloying element for the biodegradable magnesium alloy. In a newly developed ternary Mg-2Zn-0.5Nd (ZN20) alloy, Zn, as a micronutrient element, is added to improve the mechanical and corrosion properties by solution strengthening, grain refinement and increase corrosion potential of the alloy

[22,23]. Nd could weaken the texture intensity by the formation of rare earth metal texture and improve the ductility of magnesium alloy [24]. However, the performance of magnesium alloy in the reconstruction of intestinal tract and stomach is still not clear enough. The corrosion resistance plays an important role in the application of ZN20 alloy fine wire as surgical staples, because it can cause leakage once the surgical staples break due to corrosion before the reconstruction of intestinal tract and stomach, which is dangerous for the patients. And it is usually difficult to estimate whether magnesium is suitable as surgical staples only by *in vitro* study, because it is a complicated process affected by many factors after implantation in human body. Therefore, study on the potential of magnesium as surgical staples by both *in vivo* and *in vitro* experiments is necessary.

This study investigated the performance of ZN20 alloy fine wire *in vitro* and *in vivo*, evaluating its potential as surgical staples. Tensile test and bursting pressure test were carried out to examine whether it could provide sufficient mechanical support as surgical staples after anastomosis. The corrosion behavior of ZN20 alloy fine wire was studied by immersion test and SEM observation. The biological property of fine ZN20 alloy wire was studied by biochemical test and histological analysis after implantation *in vivo*.

2. Materials and methods

2.1. Materials

ZN20 alloy fine wires, with 0.3 mm in diameter, were obtained by combing drawing with annealing from an initial diameter of 10 mm. The drawing was carried out by a hydraulic drawing machine and diamond mold at room temperature with a drawing speed of 25 mm s^{-1} and area reduction of 6–9% per pass. The accumulative AR between two annealing was 20%, and the annealing was carried out at 300 °C for 0.5 h. ZN20 alloy was annealed at 300 °C for 0.5 h after it was drawn to 0.3 mm. Lubricating grease was used to reduce the friction during drawing and improve the surface quality. Ultrasonic cleaning with acetone and alcohol was carried out to eliminate the residues from the lubricating grease on the surface of wire after drawing.

2.2. Microstructure

Optical microscope (OLYMPUS-GX7) was used to observe the longitudinal microstructure of the ZN20 alloy wire. ZN20 alloy fine wires were embedded into epoxy resin, then grounded with SiC papers up to 2000 grid, polished by diamond paste and etched by an etching solution (6 g picric acid, 10 mL acetic acid, 10 mL distilled water and 70 mL absolute ethanol). Afterward, ZN20 alloy wire was rinsed with ethyl alcohol and dried in air. The second phase of fine ZN20 alloy wire was identified by X-ray diffraction (XRD) after ranging several wires along drawing direction to form a dimension of 10 mm ×10 mm.

2.3. Tensile test

Tensile properties of the wire were measured on a universal testing machine (ZwickZ050) with a tensile speed of 1 mm min^{-1} at room temperature. The gauge length and diameter of the wire specimen were 100 and 0.3 mm, respectively. At least three specimens were tested for each time to obtain reliable results.

2.4. Surgical staples anastomosis in vitro

ZN20 alloy fine wire was processed into U-shape surgical staples that were loaded in circumcision stapler. The circumcision stapler then deformed the surgical staples from U-shape to B-shape. Scanning electron microscope (SEM) (Zeiss Supra 55) was used to observe the surface morphology of the wire after anastomosis.
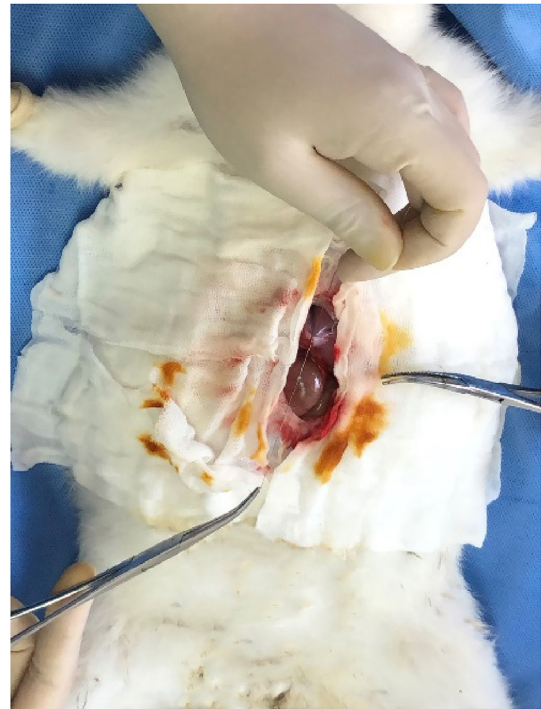

Fig. 1. The surgical procedure of knotting on stomach.

2.5. Bursting pressure test

ZN20 alloy fine wire was machined into U-shaped surgical staples that were loaded in circumcision stapler. The intestine of pig was cut into two pieces, anastomosed by a circumcision stapler (Waston GLT-34-C/D) loaded with 32 ZN20 surgical staples. Intestine tract was filled with water at a constant speed after connecting with a pressure detecting device. The maximum pressure was recorded before the intestine burst. This measurement was repeated at least 3 times to give an average of the results.

2.6. Corrosion test in vitro

ZN20 alloy wire was cut into 1 cm length and then cleaned ultrasonically by acetone and alcohol. The pH of simulated stomach fluid is 1.2 (acidic), magnesium will degrade quickly after immersed in such simulated stomach fluid. Considering the environment of intestine and stomach, simulated intestine fluid was chose as the corrosion medium for immersion test, because the simulated stomach fluid is too corrosive for magnesium. The simulated intestinal fluid was prepared according to the pharmacopeia of United States, using 6.8 g KH$_2$PO$_4$ and 500 mL distill water. The pH of the fluid was adjusted to 6.8 by NaOH with concentration of 0.2 mol L^{-1}, and finally distill water was added to ensure that the volume of the solution was 1000 mL. ZN20 alloy wire was immersed in the simulated intestinal fluid with a ratio of 20 mL cm^{-2} according to ASTM-G31-72 at 37 °C for 7 days. The solution was freshly changed every day, and the concentration of magnesium ions was measured by Optima 7300DV inductively coupled plasma atomic emission spectrometer (ICP-AES, PE, USA). The corrosion rate of the wire was calculated as below:

$$C = K \times W / \rho / A / t$$

where K is a constant (8.76 × 10^4), W is the weight loss of the wire after immersed in simulated intestine fluid (g), ρ is the density of ZN20 alloy (g cm^{-3}), A is the surface area of the wire (cm^2), t is the immersion time (h). And the weight loss was calculated as follows:
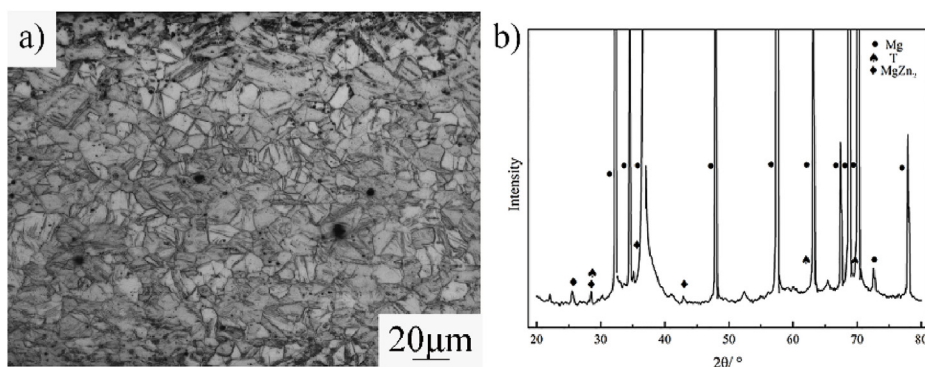
$$W = c \times V \times M$$

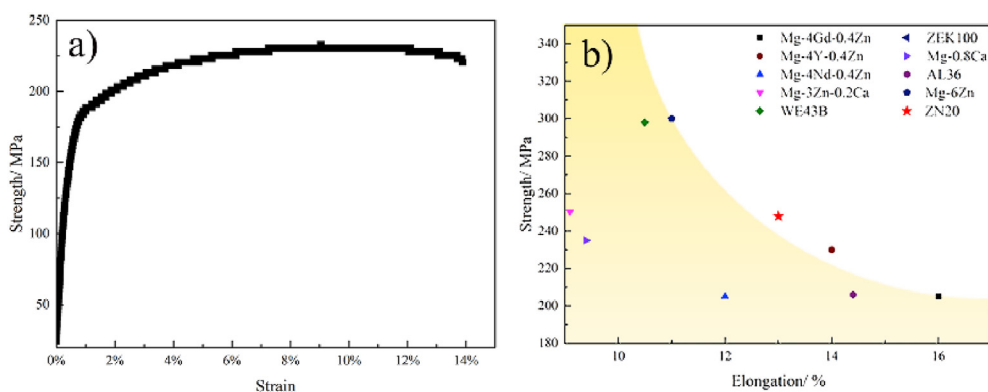**Fig. 2.** Microstructure (a) and XRD patterns (b) of ZN20 fine wires.

Fig. 3. The stress-strain curves of the experimental ZN20 alloys at room temperature (a) and comparison of ultimate tensile strength vs. elongation for present ZN20 alloy wires and recent developed magnesium alloy wires (b) [25–29].
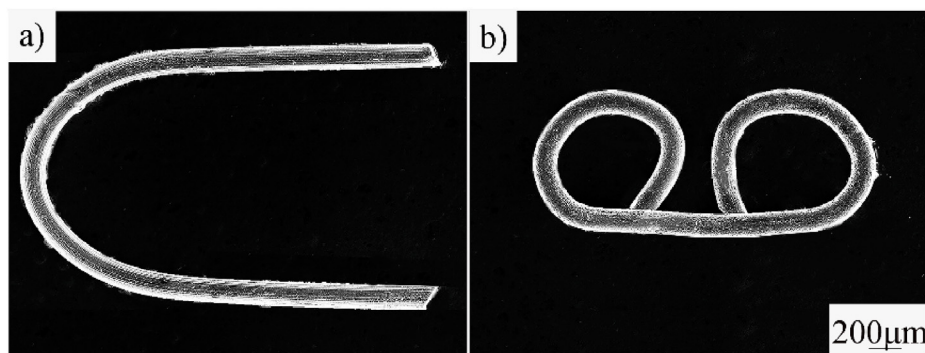

Fig. 4. Optical microstructure of ZN20 alloy wires (a) and morphology of ZN20 alloy surgical staples: (b) U-shaped; (c) B-shaped.
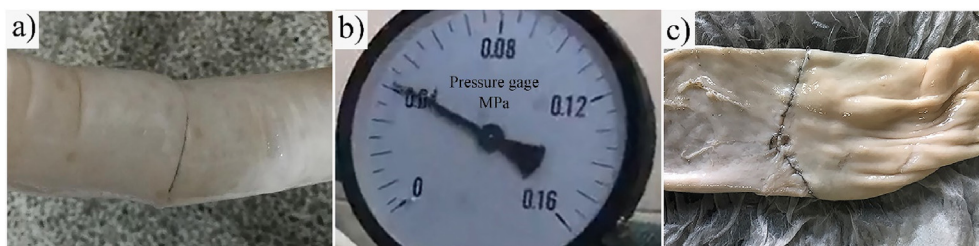

Fig. 5. Intestine of pig before (a) and after (c) bursting pressure test and the pressuring device until intestine break.

where c is Mg^{2+} concentration (mol L^{-1}), V is the volume of simulated intestinal fluid during immersion test (L) and M is molar mass of magnesium (g mol^{-1}). A scanning electron microscope (SEM, Zeiss Supra 55) equipped with Energy Dispersive Spectroscopy (EDS) was used to observe the corrosion morphology of the wire after corrosion in the simulated intestine fluid. The corroded wire was embedded into epoxy resin, which was grounded to 2000 grid and polished by diamond paste.
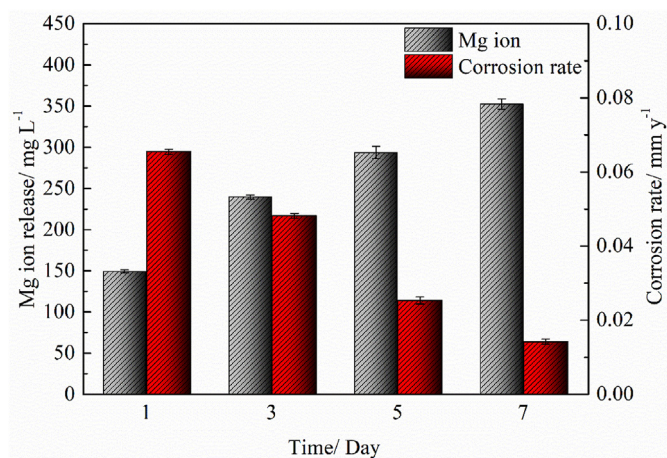
Fig. 6. Accumulative Mg ion release and corrosion rate of ZN20 alloy wires during immersion test in the simulated intestine fluid up for 7 days.

2.7. Animals test

The animal test was approved by the Ethics Committee of General Hospital of Northern Theater Command, Shenyang, designed according to the Guide for the Care and Use of Laboratory Animals issued by the Ministry of Science and Technology of China. 12 female New Zealand rabbits with weight of about 3.0 kg were used as the experimental animals.

The surgery was operated under sterile condition, and all the instruments and the materials were sterilized. Intraperitoneal injection of chloral hydrate was carried out to anesthetize the animal. A median incision was cut to expose the intestine and stomach of the rabbits. The intestine and stomach were drug out by using suture line, as shown in Fig. 1. Then ZN20 alloy fine wire was knotted on the intestine and stomach respectively. Finally, the abdomen was closed layer by layer. Penicillin was subcutaneously injected to relieve the inflammation for 3 days after implantation. The rabbits were divided into four groups as time intervals.

After implantations for 1, 2, 4 and 8 weeks, respectively, 1.5 mL of venous blood was obtained from the auricular vein, and placed in sterile tubes with anticoagulant. Automatic blood biochemistry analyzer (Hitachi 7600-020, Japan; reagent was provided by Koch Industries, USA) was used to detect the concentration of serum magnesium, glutamic–pyruvic–transaminase (GPT), glutamic–oxaloacetic–transaminase (GOT), blood urea nitrogen (BUN), and creatinine (CREA).

The animals were sacrificed after 1, 2, 4 and 8 weeks' implantation, and the tissues with ZN20 alloy fine wire were removed and immersed in 10% buffered formaldehyde. Then the tissue was embedded in xylene and paraffin after dehydration, stained with hematoxylin and eosin (HE), and observed by an optical microscope (Scope.A1, ZEISS). The remaining wires were brought to observe their morphologies after dehydration and gold-spraying by SEM equipped with EDS.

3. Results

3.1. Tensile properties and surgical staple anastomosis in vitro

Fig. 2 is the microstructure and XRD patterns of the ZN20 alloy wires. The average grain size of ZN20 alloy wires was 10 μm. And $MgZn_2$ and $Mg_{60}Zn_{32}Nd_8$ phase can be identified that existed in ZN20 alloy wires based on the results of Fig. 2b. Fig. 3 shows mechanical property of ZN20 alloy wires in this study and some typical Mg alloy wires in recent studies [25–29]. These magnesium alloy wires exhibit two characteristics: high strength with lower ductility or good ductility with lower strength. ZN20 alloy wires in this study exhibited an excellent comprehensive mechanical property. The ultimate tensile strength (UTS) of the wire was about 248 ± 8 MPa, which is higher than the standard regulated by YY 0875-2013, indicating that it can provide certain mechanical support after anastomosis. The elongation of the wire was 13 ± 0.72%, implying that its' good formability when deformed from U-shape to B-shape. Fig. 4 is the surface morphology of ZN20 alloy staples before and after anastomosis. And there was no crack on the surface after anastomosis, and the wire could maintain its surface integrity, which illustrated the good formability of the ZN20 alloy fine wire.
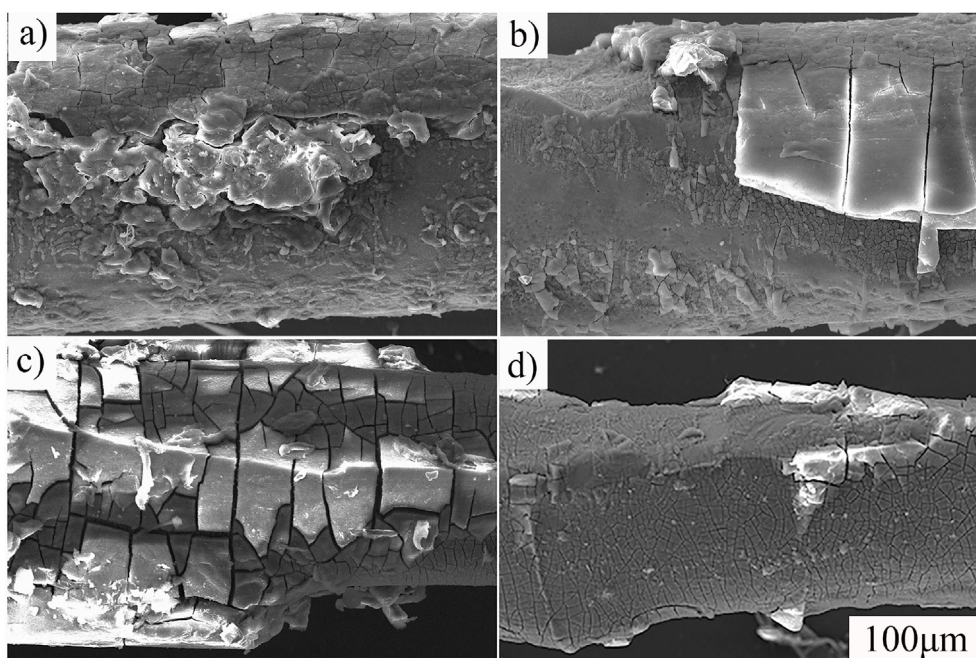

Fig. 7. Corrosion morphologies of ZN20 alloy wires after immersion in simulated intestine fluid for different days: (a) 1 day; (b) 3 days; (c) 5 days and (d) 7 days.
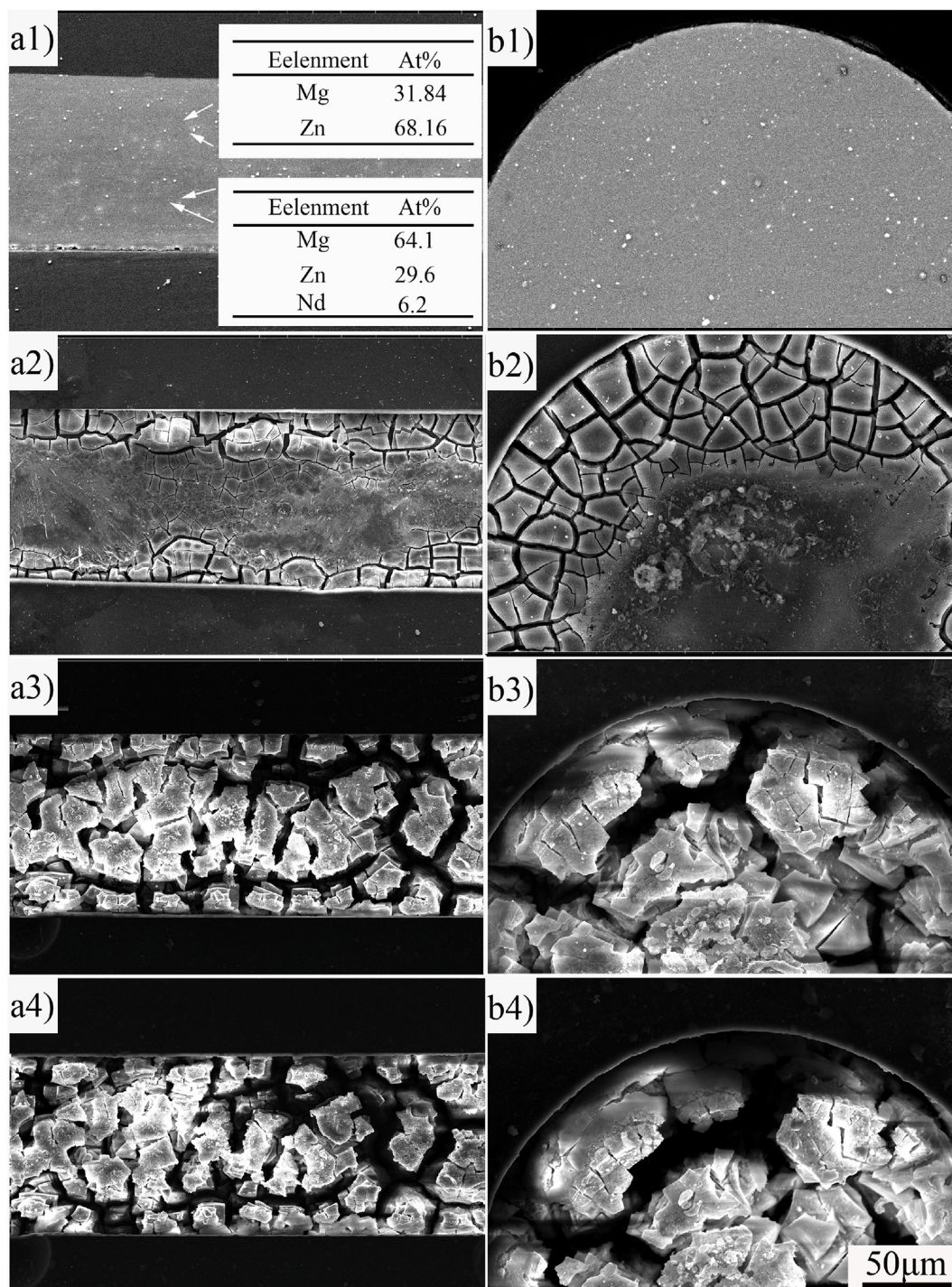
Eelenment	At%
Mg	31.84
Zn	68.16

Eelenment	At%
Mg	64.1
Zn	29.6
Nd	6.2

Fig. 8. Corrosion morphologies of ZN20 alloy wire immersed in simulated intestine fluid for up to 72 h: (a) longitudinal sectional; (b) cross sectional; (1) 0 h; (2) 6 h; (3) 60 h; (4) 72 h.

3.2. Surgical staple anastomosis in vitro

Fig. 5 shows the intestine of pig anastomosed by ZN20 alloy staples, before and after bursting pressure test, and the pressure until the intestine break. After the intestine of pig was anastomosed by a circumcision stapler with ZN20 alloy staples, it was filled with water at a constant speed. There was no leakage after the intestine was filled with water (Fig. 5a). The pressure was about 40 kPa when the pig intestine bursting (Fig. 5b), which is nearly 11 times greater than the bursting pressure regulated by general technical conditions for stapler in YY 0245-2008. This indicates that ZN20 alloy surgical staples can provide sufficient mechanical support after anastomosis. When the pig intestine burst at 40 kPa, only the intestine broke and ZN20 alloy staples were still in good condition (Fig. 5c).

3.3. Corrosion of wires in vitro

To investigate the corrosion resistance of ZN20 alloy fine wires, immersion test was carried out in the simulated intestine fluid at 37 °C for 7 days. Fig. 6 shows the accumulative Mg ion release and corrosion rate of ZN20 alloy wire after immersion in the simulated intestine fluid for 7 days. The accumulative Mg ion release after 1, 3, 5 and 7 days
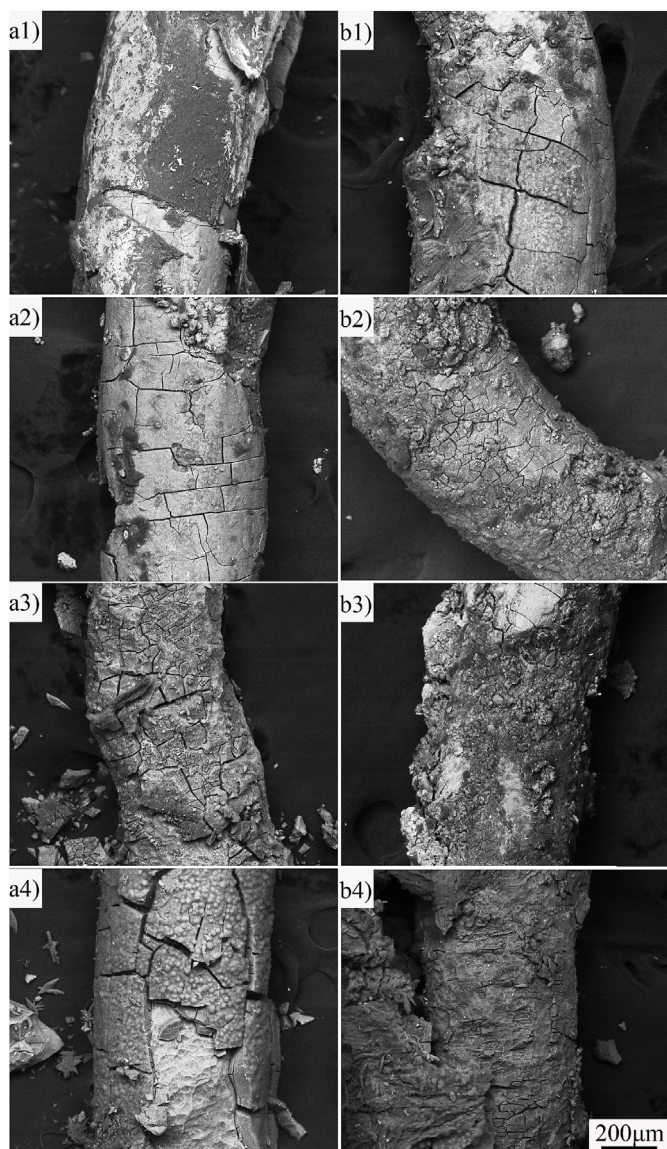
Fig. 9. Corrosion morphologies of ZN20 alloy wires taken out from the tissue of the rabbits after 2 months implantation: (a) implant in intestine; (b) implant in stomach; (1) 1 week; (2) 2 weeks; (3) 4 weeks; (4) 8 weeks.

were 149, 240, 294 and 353 mg L^{-1}, respectively. The results showed that ZN20 alloy wire corroded severely at the early stage. As can be seen in Fig. 6, the corrosion rate decreased with the immersion time. And the amount of Mg ions in the simulated intestine fluid increased continually as the wire corroded with the immersion time. The corrosion product deposited on the surface of ZN20 alloy wire increased continuously with the immersion time. And the corrosion product layer will decrease the corrosion rate by protecting the wire from the simulated intestine fluid.

Fig. 7 shows corrosion morphologies of ZN20 alloy fine wires after 7 days immersion in the simulated intestinal fluid without removing the corrosion products. There were two obvious changes during the 7 days immersion. Firstly, corrosion product formed on the surface of ZN20 alloy wire as it interacted with the simulated intestine fluid (Fig. 7a). Then the outer layer began to peel off as the immersion time was prolonged (Fig. 7c).

To investigate the corrosion mechanism of ZN20 alloy fine wires in the simulated intestine fluid, the corrosion morphology was observed by SEM. Fig. 8 shows the corrosion morphologies of ZN20 alloy wire immersed in the simulated intestine fluid for up to 72 h observed by

SEM *in situ*. The composition of second phase was confirmed by EDS analysis. Based on the XRD patterns of ZN20 alloy and EDS analysis shown in Fig. 8a1, it can be suggested that ZN20 alloy wires were consisted of smaller granular $MgZn_2$ phases and bigger granular $Mg_{60}Zn_{32}Nd_8$ phases. The corrosion crack first appeared at the outside layer of the wire (Fig. 8a2, Fig. 8b2), then it gradually spread to the center of the wire (Fig. 8a3, Fig. 8b3). Finally, continuous corrosion cracking was formed on the outside of the wire as the corrosion continued to extend, which eventually led to the peeling and fracture of the ZN20 alloy wire during immersion in the simulated intestinal fluid (Fig. 8a4, Fig. 8b4).

3.4. Corrosion of wires in vivo

Fig. 9 shows the corrosion morphologies of ZN20 alloy fine wires *in vivo* taken out from the tissue of the rabbits after 2 months implantation. The characteristic of the corrosion response of the wires *in vivo* was similar to that *in vitro*. Corrosion crack appeared on the surface of the wires at early stage after implantation (Fig. 9a2, Fig. 9b1). Then the outside layer of the wire began to peel off as the corrosion crack extended to the other part of the wire (Fig. 9a4, Fig. 9b4). The peeling off in Fig. 9b4 was more serious than that in Fig. 9a4, which illustrates that the corrosion rate in stomach should be faster than that in intestine.

3.5. Biochemical behavior

Biochemical tests were carried out to investigate the biocompatibility of ZN20 alloy fine wires as surgical staples. Fig. 10 shows blood biochemical indicators (Aspartate Aminotransferase (AST), Alanine Aminotransferase (ALT), Urea, Creatinine and Mg) after the implantation for different times. After implantation, the serum Mg stayed at a stable level (Fig. 10e), indicating that Mg can be absorbed and metabolized *in vivo*. Although AST and ALT values after implantation for 4 weeks were slightly higher than those before implantation ($P = 0.228$, $P = 0.792$), no significant difference was observed between them (Fig. 10a and b). Same results occurred in the indicators of UREA and CREA. Although there were some differences in UREA and CREA values between pre-implantation and post implantation after 4 weeks ($P = 0.271$, $P = 0.259$), there was no statistically significant difference between them (Fig. 10c and d).

3.6. Histological evaluation

HE staining histologic images in Fig. 11 show no dynamic inflammatory cell infiltration in both stomach (Fig. 11a) and intestine (Fig. 11b). The gastric and intestinal tissue exhibited normal morphology after 8 weeks implantation. These pathological results demonstrated that the degradation of ZN20 alloy fine wires did not cause damage to both intestine and stomach.

4. Discussion

The above experimental results indicate that the corrosion rate of ZN20 alloy *in vitro* decreased with the immersion time under the influence of formation of corrosion product on the surface. The mechanical properties and bursting pressure of ZN20 alloy fine wire meet the requirement of YY 0875-2013 and YY 0245-2008, and it can supply sufficient mechanical support after anastomose. The results of both biochemical and pathology tests showed the biocompatibility and biological safety of ZN20 alloy fine wires. The wire would break after 3 days immersion in the simulated intestine fluid *in vitro*. Whereas it could exist for 2 months after implantation in the stomach, where is very corrosive to magnesium alloys. The discrepancy of the corrosion rate *in vitro* and *in vivo* needs to discuss in detail.

Based on the corrosion morphology of ZN20 alloy fine wires immersed in simulated intestine fluid for 72 h (Fig. 8), a schematic
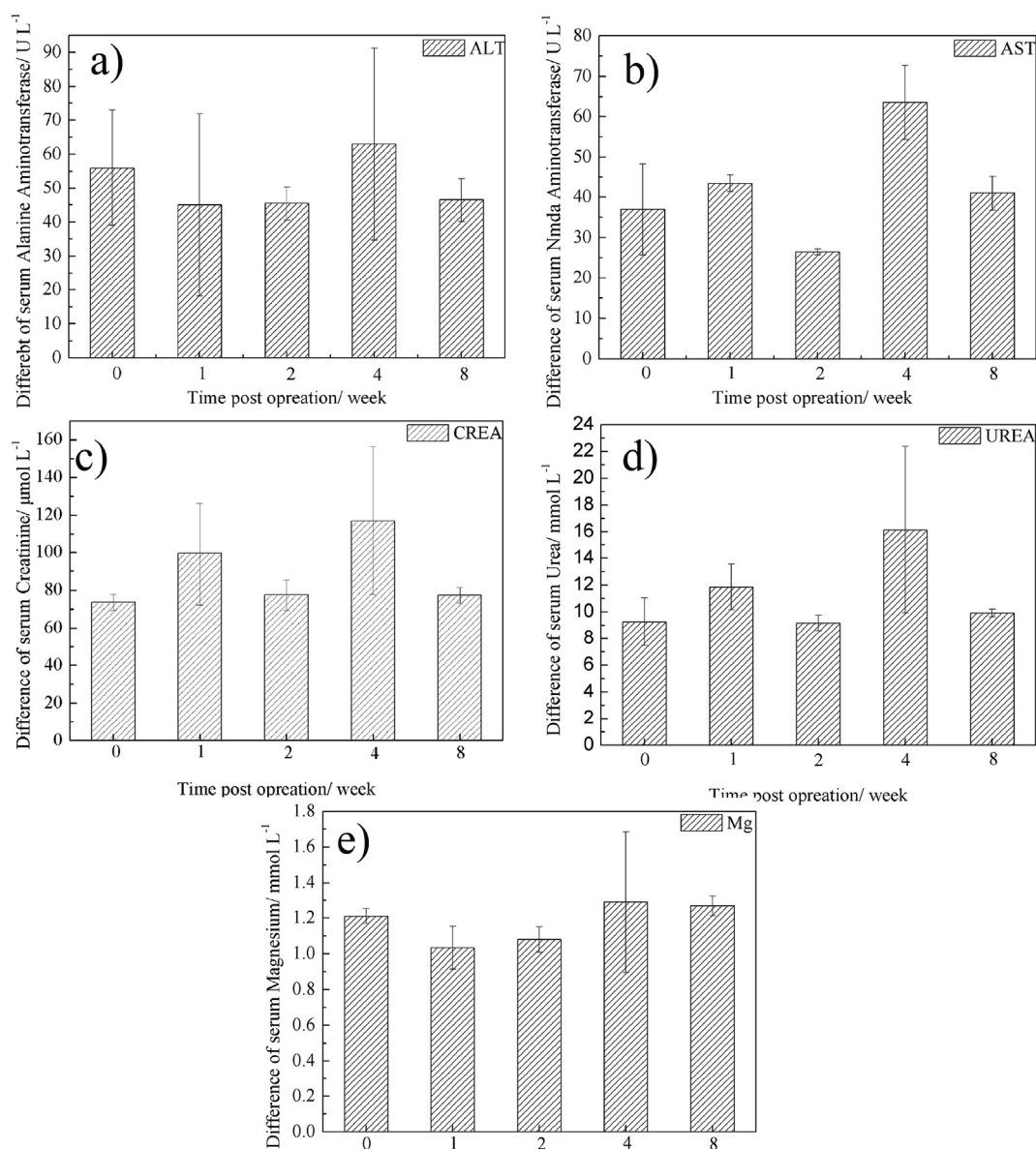
Fig. 10. Blood biochemical indicators (difference of the values between pre- and post-implantation): (a) ALT; (b) AST; (c) CREA; (d) UREA; (e) magnesium.
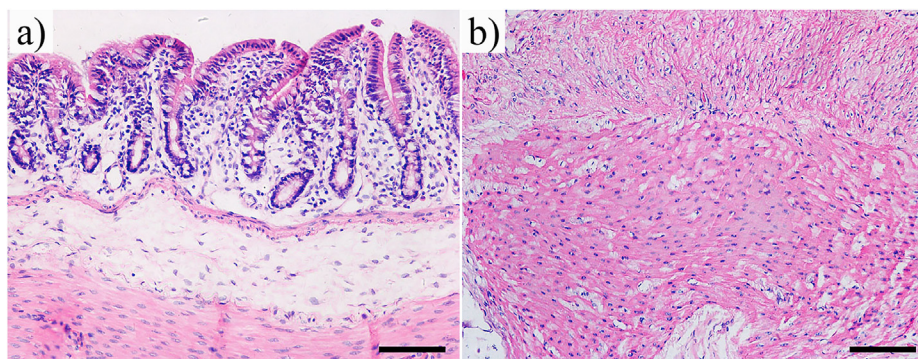

Fig. 11. Histological images after 8 weeks implantation (hematoxylin–eosin staining, ×200): (a) intestine; (b) stomach.

illustration is given in Fig. 12 to further explain the corrosion behavior of the wire *in vitro*. At stage I, the corrosion mainly occurred on the outside layer of the wire. The residual tension, which has a bad influence on corrosion resistance, was usually formed on the outside of the wire during drawing along axial direction and circumferential direction

[30,31]. Therefore, the corrosion should first appear on the outside of ZN20 alloy wire as it contacted the simulated intestine fluid. At stage II, galvanic corrosion occurred as the corrosion extended to the internal of ZN20 alloy wire. Cai [32] reported that $MgZn_2$ phase has a relative Volta potential of about +550 mV, acting as a micro-cathode during
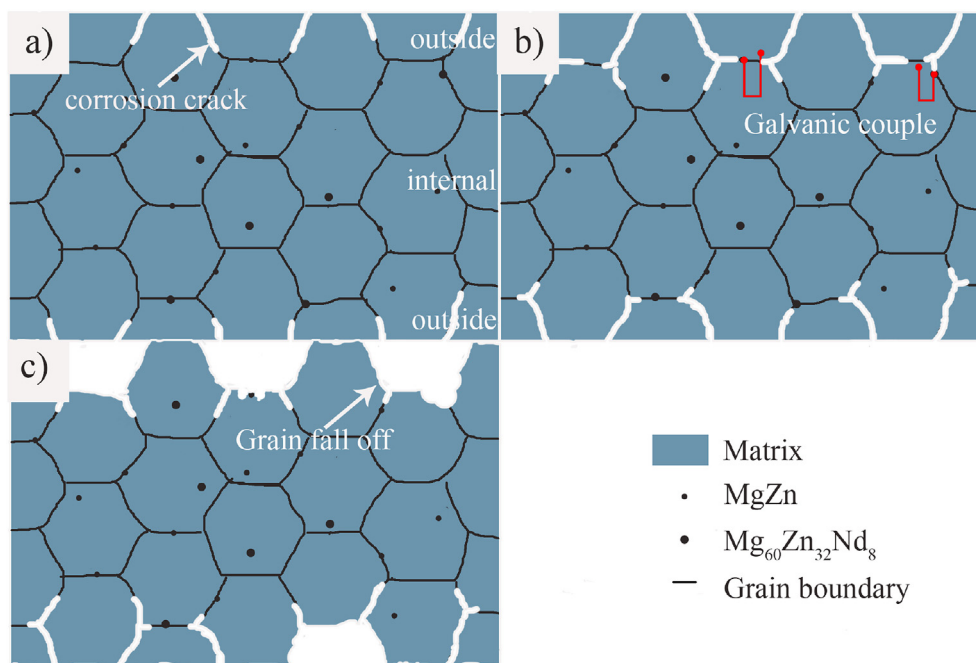
Fig. 12. Schematic illustration of corrosion behavior of ZN20 alloy wire.
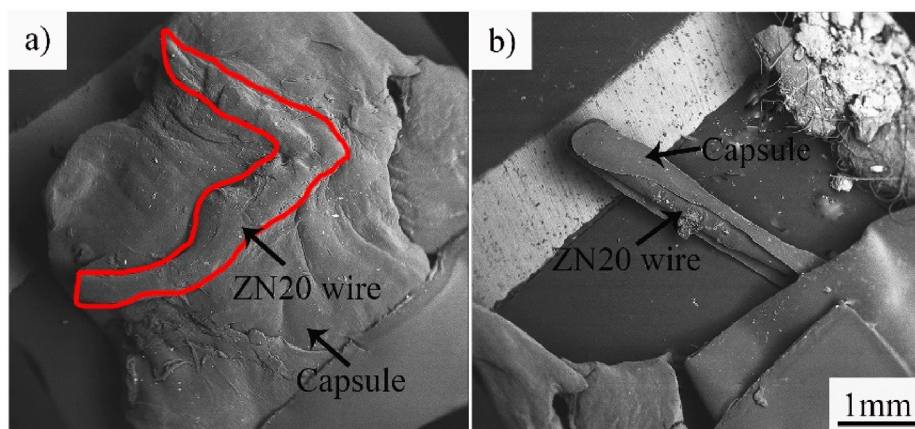

Fig. 13. The capsule observed on the surface of ZN20 alloy wire after 8 weeks' implantation: (a) implant in stomach; (b) implant in intestine.

the corrosion process in simulated intestine fluid. While the $Mg_{60}Zn_{32}Nd_8$ phase has about -400 mV of relative Volta potential, acting as a micro-anode to be corroded preferentially. The Mg matrix around $MgZn_2$ phases dissolved as the anode, while $Mg_{60}Zn_{32}Nd_8$ phases dissolved as the anode at same time. At stage III, grains began to peel off when continuous corrosion cracks appeared.

ZN20 alloy fine wires peeled off after immersion in simulated intestine fluid for 3 days, and the wire diameter decreased on the 3rd day *in vitro*, while the decrease in diameter appeared after 2 months implantation *in vivo*. The environment *in vivo* is more complicated than *in vitro*, and the tissue reaction started as ZN20 alloy fine wire was implanted, which did not exist in the immersion *in vitro*. Fibroblasts and macrophages should rapidly attach to the surface of fine ZN20 alloy wire [33]. Then a capsule (newly generated tissue), which could protect ZN20 alloy fine wire from interaction with physiological salt solution, was observed on the surface of the wire (Fig. 13). Therefore, the corrosion rate *in vitro* was faster than that *in vivo*.

5. Conclusions

ZN20 alloy fine wires with diameter of 0.3 mm were prepared by multi-passes cold drawing combined with annealing. Mechanical properties, bursting pressure, biodegradation *in vitro* and *in vivo* were studied in order to evaluate the potential of ZN20 alloy fine wires as surgical staples. The following conclusions are obtained:

The bursting pressure of ZN20 alloy fine wire was about 40 kPa, which is nearly 11 times of the standard in YY 0245-2008 for the stapler.

Biochemical test and pathology analysis revealed that ZN20 alloy fine wire has good biocompatibility and biological safety.

The corrosion resistance of ZN20 alloy fine wire *in vivo* was higher than that *in vitro* mainly due to the capsule formed on the surface of the wire.

Declaration of interests

The authors declare no competing financial interest.

CRediT authorship contribution statement

Ming Gao: Conceptualization, Methodology, Validation, Software, Formal analysis, Investigation, Writing - original draft, Writing - review

& editing. **Di Na:** Methodology, Validation, Formal analysis, Investigation. **Xiangqiao Ni:** Methodology, Investigation, Formal analysis. **Lihui Song:** Investigation, Data curation. **Iniobong P. Etim:** Writing - review & editing. **Ke Yang:** Writing - review & editing. **Lili Tan:** Supervision, Project administration, Conceptualization, Funding acquisition, Writing - review & editing. **Zheng Ma:** Supervision, Conceptualization, Writing - review & editing.

Acknowledgement

References

[1] T.A.G. Donato, L.H. de Almeida, R.A. Nogueira, T.C. Niemeyer, C.R. Grandini, R. Caram, S.G. Schneider, A.R. Santos, Cytotoxicity study of some Ti alloys used as biomaterial, Mat. Sci. Eng. C Bio. S. 29 (4) (2009) 1365–1369, https://doi.org/10.1016/j.msec.2008.10.021.

[2] S. Demertzis, O. Beslac, D. Mettler, D. Zalokar, T. Spangler, B. Hausen, L. Swanstrom, Beyond the "B": a new concept of the surgical staple enabling miniature staplers, Surg. Endosc. 29 (12) (2015) 3674–3684, https://doi.org/10.1007/s00464-015-4125-x.

[3] A. Mohammad, R. Hang, C. Wang, Z. Yu, Z. Li, Y. Xiao, Biodegradable metallic wires in dental and orthopedic applications: a review, Metals 8 (4) (2018) 212–244, https://doi.org/10.3390/met8040212.

[4] H. Wu, C. Zhao, J. Ni, S. Zhang, J. Liu, J. Yan, Y. Chen, X. Zhang, Research of a novel biodegradable surgical staple made of high purity magnesium, Bioact. Mater. 1 (2) (2016) 122–126, https://doi.org/10.1016/j.bioactmat.2016.09.005.

[5] P.K. Bowen, J. Drelich, J. Goldman, Magnesium in the murine artery: probing the products of corrosion, Acta Biomater. 10 (3) (2014) 1475–1483, https://doi.org/10.1016/j.actbio.2013.11.021.

[6] Y.F. Ding, C.E. Wen, P. Hodgson, Y.C. Li, Effects of alloying elements on the corrosion behavior and biocompatibility of biodegradable magnesium alloys: a review, J. Mater. Chem. B 2 (14) (2014) 1912–1933, https://doi.org/10.1039/C3TB21746A.

[7] A. Alabbasi, M.B. Kannan, C. Blawert, Dual layer inorganic coating on magnesium for delaying the biodegradation for bone fixation implants, Mater. Lett. 124 (2014) 188–191, https://doi.org/10.1016/j.matlet.2014.03.094.

[8] R. Waksman, R. Pakala, P.K. Kuchulakanti, R. Baffour, D. Hellinga, R. Seabron, F.O. Tio, E. Wittchow, S. Hartwig, C. Harder, R. Rohde, B. Heublein, A. Andreae, K.H. Waldmann, A. Haverich, Safety and efficacy of bioabsorbable magnesium alloy stents in porcine coronary arteries, Cathet. Cardiovasc. Interv. 68 (4) (2006) 607–617, https://doi.org/10.1002/ccd.20727.

[9] C.B. Chng, D.P. Lau, J.Q. Choo, C.K. Chui, A bioabsorbable microclip for laryngeal microsurgery: design and evaluation, Acta Biomater. 8 (7) (2012) 2835–2844, https://doi.org/10.1016/j.actbio.2012.03.051.

[10] Waksman Ron, Erbel Raimund, Mario Carlo Di, Early- and long-term intravascular ultrasound and angiographic findings after bioabsorbable magnesium stent implantation in human coronary arteries, JACC Cardiovasc. Interv. 2 (4) (2009) 312–320, https://doi.org/10.1016/j.jcin.2008.09.015.

[11] W. Wang, K.C. Nune, L. Tan, N. Zhang, J. Dong, J. Yan, R.D.K. Misra, K. Yang, Bone regeneration of hollow tubular magnesium strontium scaffolds in critical-size segmental defects: effect of surface coatings, Mat. Sci. Eng. C Mater. 100 (2019) 297–307, https://doi.org/10.1016/j.msec.2019.02.067.

[12] F. Witte, V. Kaese, H. Haferkamp, E. Switzer, H. Windhagen, In vivo corrosion of four magnesium alloys and the associated bone response, Biomaterials 26 (17) (2005) 3557–3563, https://doi.org/10.1016/j.biomaterials.2004.09.049.

[13] M. Li, W.D. Wang, Y. Zhu, Y. Lu, P. Wan, K. Yang, Y. Zhang, C.B. Mao, Molecular and cellular mechanisms for zoledronic acid-loaded magnesium-strontium alloys to inhibit giant cell tumors of bone, Acta Biomater. 77 (2018) 365–379, https://doi.org/10.1016/j.actbio.2018.07.028 https://search.crossref.org/?q=M.+Li%2C+W.D.+Wang%2C+Y.+Zhu%2C+Y.+Lu%2C+P.+Wan%2C+K.+Yang%2C+Y.+Zhang%2C+C.B.+Mao%2C+Molecular+and+cellular+mechanisms+for+zoledronic+acid-loaded+magnesium-strontium+alloys+to+inhibit+giant+cell+tumors+of+bone.+Acta+Biomater..+77+%282018%29+365-379.

[14] K.M. Burgazli, N.I. Stein, M. Mericliler, M. Parahuleva, A. Erdogan, Influence of HMG-CoA reductase inhibitors on leptin-induced endothelial cell proliferation, migration, and capillary-like tube formation, Postgrad. Med. 126 (3) (2014) 231–238, https://doi.org/10.3810/pgm.2014.05.2771.

[15] B. Daniela, N. Anna, M. Andrzej, A.M.M. Jeanette, Magnesium and microvascular endothelial cells: a role in inflammation and angiogenesis, Front. Biosci. 10 (1–3) (2005) 1177–1182, https://doi.org/10.2741/1610.

[16] C. Jian, K.-W. Jiang, X.-D. Yang, Z.-L. Shen, S. Wang, Animal experimental study of biodegradable magnesium alloy stapler for gastrointestinal anastomosis, Chin. J. Gastrointest Surg. 16 (8) (2013) 772–776, https://doi.org/10.3760/cma.j.issn.1671-0274.2016.08.018.

[17] R. Xu, X. Yang, K.W. Suen, G. Wu, P. Li, P.K. Chu, Improved corrosion resistance on biodegradable magnesium by zinc and aluminum ionimplantation, Appl. Surf. Sci. 263 (2012) 608–612, https://doi.org/10.1016/j.apsusc.2012.09.116.

[18] A.C.W. Noorakma, Hussain Zuhailawati, Hydroxyapatite-coated magnesium-based biodegradable alloy: cold spray deposition and simulated body fluid studies, J. Mater. Eng. Perform. 22 (10) (2013) 2997–3004, https://doi.org/10.1142/9789814322799_0062.

[19] Z. Jing, Y. Gu, Y. Guo, C. Ning, Electrochemical behavior of biocompatible AZ31 magnesium alloy in simulated body fluid, J. Mater. Sci. 47 (13) (2012) 5197–5204, https://doi.org/10.1007/s10853-012-6403-5.

[20] S. El-Rahman, Neuropathology of aluminum toxicity in rats (glutamate and GABA impairment), Pharmacol. Res. 47 (3) (2003) 189–194, https://doi.org/10.1016/S1043-6618(02)00336-5.

[21] C.H. Ku, D.P. Pioletti, M. Browne, P.J. Gregson, Effect of different Ti-6Al-4V surface treatments on osteoblasts behaviour, Biomaterials 23 (6) (2002) 1447–1454, https://doi.org/10.1016/S0142-9612(01)00266-6.

[22] C.G. Fraga, Relevance, essentiality and toxicity of trace elements in human health, Mol. Aspect. Med. 26 (4–5) (2005), https://doi.org/10.1016/j.mam.2005.07.013 0-244.

[23] Y.a. Chen, L. Jin, Y. Song, H. Liu, R. Ye, Effect of Zn on microstructure and mechanical property of Mg–3Sn–1Al alloys, Mater. Sci. Eng. A Struct. 612 (33) (2014) 96–101, https://doi.org/10.1016/j.msea.2014.06.02.

[24] J. Bohlen, S. Yi, D. Letzig, K.U. Kainer, Effect of rare earth elements on the microstructure and texture development in magnesium–manganese alloys during extrusion, Mater. Sci. Eng. A Struct. 527 (26) (2010) 7092–7098, https://doi.org/10.1016/j.msea.2010.07.081.

[25] L. Sun, J. Bai, F. Xue, L. Tao, C. Chu, J. Meng, Exceptional texture evolution induced by multi-pass cold drawing of magnesium alloy, Mater. Des. 135 (2017) 267–274, https://doi.org/10.1016/j.matdes.2017.09.027.

[26] A.J. Griebel, J.E. Schaffer, T.M. Hopkins, A. Alghalayini, T. Mkorombindo, K.O. Ojo, Z. Xu, K.J. Little, S.K. Pixley, An in vitro and in vivo characterization of fine WE43B magnesium wire with varied thermomechanical processing conditions, J. Biomed. Mater. Res. B Appl. Biomater. 106 (5) (2018) 1987–1997, https://doi.org/10.1002/jbm.b.34008.

[27] J. Bai, L. Yin, Y. Lu, Y. Gan, F. Xue, C. Chu, J. Yan, K. Yan, X. Wan, Z. Tang, Preparation, microstructure and degradation performance of biomedical magnesium alloy fine wires, Prog. Nat. Sci. Mater. 24 (5) (2014) 523–530, https://doi.org/10.1016/j.pnsc.2014.08.015.

[28] M. Zheng, G. Xu, D. Liu, Y. Zhao, B. Ning, M. Chen, Study on the microstructure, mechanical properties and corrosion behavior of Mg-Zn-Ca alloy wire for biomaterial application, J. Mater. Eng. Perform. 27 (4) (2018) 1837–1846, https://doi.org/10.1007/s11665-018-3278-x.

[29] J.-M. Seitz, D. Utermöhlen, E. Wulf, C. Klose, F.-W. Bach, The manufacture of resorbable suture material from magnesium - drawing and stranding of thin wires, Adv. Eng. Mater. 13 (12) (2011) 1087–1095, https://doi.org/10.1002/adem.201100152.

[30] Y. Zhang, J You, J. Lu, C. Cui, Y. Jiang, X. Ren, Effects of laser shock processing on stress corrosion cracking susceptibility of AZ31B magnesium alloy, Surf. Coating. Technol. 204 (24) (2010) 3947–3953, https://doi.org/10.1016/j.surfcoat.2010.03.015.

[31] A. Phelippeau, S. Pommier, T. Tsakalakos, M. Clavel, C. Prioul, Cold drawn steel wires - processing, residual stresses and ductility - Part I: metallography and finite element analyses, Fatigue Fract. Eng. M 29 (3) (2010) 201–207, https://doi.org/10.1111/j.1460-2695.2005.00981.x.

[32] C. Cai, R. Song, L. Wang, J. Li, Effect of anodic T phase on surface micro-galvanic corrosion of biodegradable Mg-Zn-Zr-Nd alloys, Appl. SurSci. 462 (2018) 243–254, https://doi.org/10.1016/j.apsusc.2018.08.107.

[33] A.J. Griebel, J.E. Schaffer, T.M. Hopkins, A. Alghalayini, T. Mkorom bindo, K.O. Ojo, Z. Xu, K.J. Little, S.K. Pixley, An in vitro and in vivo characterization of fine WE43B magnesium wire with varied thermomechanical processing conditions, J. Biomed. Mater. Res. B 106 (5) (2018) 1987–1997, https://doi.org/10.1002/jbm.b.34008.